Clustered Adaptation for Estimation of Time-Varying Underwater Acoustic Channels

Zhaohui Wang, *Student Member, IEEE*, Shengli Zhou, *Senior Member, IEEE*, James C. Preisig, *Member, IEEE*, Krishna R. Pattipati, *Fellow, IEEE*, and Peter Willett, *Fellow, IEEE*

***Abstract*—In this paper, we present a sparse channel estimator that exploits channel coherence across blocks for orthogonal frequency division multiplexing (OFDM) in underwater acoustic (UWA) transmissions. We propose a novel channel variation model that the channel paths within a cluster share the same amplitude, delay, and Doppler scale variations from one block to the next, but different clusters vary independently. The variation offsets for different clusters are estimated based on the measurements on the pilot subcarriers of the current block. A hybrid channel estimator is developed that can effectively utilize both the channel knowledge from the previous block and the pilot observations of the current block. Performance results based on collected data from two experiments demonstrate that adaptation with multiple clusters outperforms that with one cluster, and that the proposed cluster-adaptation based channel estimator significantly improves the system performance relative to the pilot-based counterpart.**

***Index Terms*—Clustered adaptation, OFDM, sparse channel estimation, underwater acoustic channels.**

I. Introduction

UNDERWATER acoustic (UWA) channels are doubly selective in both time and frequency [2], [3]. The medium refractions and sea surface/bottom reflections of acoustic waves in water generate multiple transmission paths which have a considerably large delay spread due to the slow sound propagation speed. The temporal dynamics of the propagation environment and/or the platform motion introduce fast channel variation. The channel coherence time could vary from several tens of milliseconds to several tens of seconds in typical operating environments [2], [4].

Manuscript received September 18, 2011; revised February 11, 2012; accepted February 12, 2012. Date of publication March 05, 2012; date of current version May 11, 2012. The associate editor coordinating the review of this manuscript and approving it for publication was Prof. Xiang-Gen Xia. The work of Z. Wang, and S. Zhou is supported by the ONR N00014-09-1-0704 (PECASE). The work of J. C. Preisig was supported by ONR Grants N00014-07-10738 and N00014-07-10184. The research of K. Pattipati was supported by the ONR under Grant N00014-09-1-0062 and by the NSF under Grants ECCS-0931956 (CPS) and ECCS-1001445 (GOALI). The research of P. Willett was supported by the ONR under Grant N00014-10-10412. This work was presented in part at the IEEE International Conference on Signal Processing, Communications and Computing, Xi'an, China, September 2011 [1].

Z. Wang, S. Zhou, K. R. Pattipati, and P. Willett are with the Department of Electrical and Computer Engineering, University of Connecticut, Storrs, CT 06269 USA (e-mail: zhwang@engr.uconn.edu; shengli@engr.uconn.edu; krishna@engr.uconn.edu; willett@engr.uconn.edu).

J. C. Preisig is with the Department of Applied Ocean Physics and Engineering, the Woods Hole Oceanographic Institution, Woods Hole, MA 02543 USA (e-mail: jpreisig@whoi.edu).

Color versions of one or more of the figures in this paper are available online at http://ieeexplore.ieee.org.

Digital Object Identifier 10.1109/TSP.2012.2189769

There are several distinct features associated with UWA multipath channels. First, the time-varying propagation paths tend to be sparsely distributed in the delay-Doppler domain, meaning that the channel energy mainly concentrates on several delay and Doppler values. Second, the paths tend to be clustered, where there are many small paths centering around the eigen-paths associated with the medium refractions and surface/bottom bounces [5]. Third, the channel coherence time varies across clusters, as different clusters are usually generated according to different transmission routes. For example, the clusters formed by medium refractions usually have larger coherence time than those formed by surface/bottom bounces. These features have been frequently observed based on field experiments at different locations (see, e.g., [6]–[10], and see also [4] on a detailed investigation on the variation of the significant paths in each cluster). Samples of channel variations for two experiments relevant to this paper are shown in Fig. 1, where we can observe different behaviors among clusters.

Various receiver designs have been developed in the literature, with different viewpoints on the channel properties. Some example works include the following.

- For single-carrier serial transmissions, a symbol-level adaptive receiver was proposed in the seminal work [11], [12], where the channel coherence is utilized after explicit phase compensation via a second-order phase-lock-loop and an adaptive decision feedback equalizer is used to suppress the intersymbol interference (ISI).
- For single-carrier block transmissions, a block-adaptive receiver with frequency domain equalization has been proposed in [13], [14], where the channels are assumed coherent between two consecutive blocks and residual phase correction is applied after channel equalization.
- For multicarrier transmissions, a block-adaptive receiver was proposed in [15] and [16] for single transmitter scenarios and in [17] for multiple-input multiple-output (MIMO) settings. Here, a single parameter referring as the Doppler scaling factor is introduced to model the time variability of the UWA channel across blocks for each pair of transmitting and receiving elements. After Doppler compensation, the channels are assumed coherent between consecutive blocks. In [18], an initialization method is developed for the progressive receivers proposed in [19] and [20], in which a complex amplitude offset and a delay offset are used to characterize the channel variation across blocks.
- For multicarrier transmissions, a block-by-block receiver was proposed in [19] and [21]–[25], where channel estimation is done on a block-by-block basis utilizing the pilot tones multiplexed with data subcarriers [15], [21], [23], [26]. Such a block-by-block receiver did not take

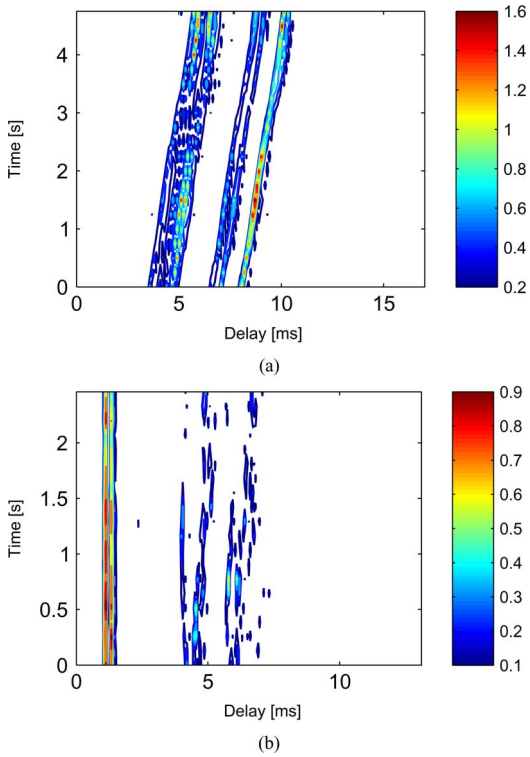

Fig. 1. Time variations of block-by-block channel estimates over 20 consecutive OFDM blocks. A constant-time (horizontal) slice across delay represents the magnitude of the channel impulse response, where the magnitude is color-coded according to color bar. No resampling is performed. (a) Mobile experiment: MACE10; (b) Stationary experiment: SPACE08.

advantage of the channel coherence between consecutive blocks. The exploitation of the channel sparsity in the delay-Doppler domain has been shown very effective for significant performance improvement [22].

The work in this paper is motivated by observing the aforementioned UWA channel characteristics and the existing receiver designs. In particular, i) the block-by-block receiver could utilize the channel coherence across blocks to reduce the number of pilots needed for channel estimation [21], [22]; ii) pilot subcarriers are beneficial for robust performance as channels do vary considerably from one block to the next; and iii) different clusters of the channels have different fluctuations, which has been recognized in the literature (e.g., [4]) but has not been effectively utilized in existing receiver designs.

In this paper, we develop a receiver for zero-padded orthogonal frequency division multiplexing (ZP-OFDM) transmissions, which incorporates clustered channel variations from one block to the next. Specifically, the channel consists of a number of distinct paths, with each path characterized by a triplet on its amplitude, delay, and Doppler scale [22]. These paths form clusters, and each cluster varies independently, assuming that paths within one cluster share three common offset parameters from one block to the next: a *group* complex attenuation factor, a *group* delay, and a *group* Doppler scaling factor. Based on the clustered channel model, we develop a two-step procedure to incorporate the channel estimate of the preceding block into the channel estimation of the current block. In the first step, the offsets of each cluster are estimated and compensated based on the channel estimate of the previous block and the received signal of the current block. In the second step, a hybrid sparse channel estimation is carried out with the input of the compensated channel parameters of each cluster and the received signal of the current block, where the cluster locations (we denote the location of each cluster as a *zone*) identified from the previous channel estimate are used to reduce the number of unknowns. After symbol detection and channel decoding in the traditional receiver, the channel estimate is refined and passed to the next block.

The proposed receiver design is developed for OFDM transmissions; however, the concept of clustered channel variations can be applied to single carrier block transmissions, e.g., [13], [14], [27], and [28]. Performance of the proposed channel estimation scheme is validated with data collected from two field experiments held off the coast of Martha's Vineyard, MA, in 2008 and 2010, respectively. The experimental result shows that i) with a moderate number of pilot symbols, the proposed channel estimator considerably outperforms its pilot-based block-by-block counterpart [21], [22], ii) adaptation using multiple clusters is beneficial relative to treating all paths as one cluster, which agrees well with the assumed physical characteristic of the channel, and iii) utilizing the zone information of clusters in channel estimation improves the system performance by limiting the search space on the unknown channel parameters.

The reminder of this paper is organized as follows. In Section II, we present a basic system model for OFDM in UWA transmissions. Based on a dynamic channel model with clustered adaptation, a block-by-block receiver design is developed in Section III. Detailed descriptions of the proposed receiver structure, including estimation of the channel variations and a hybrid sparse channel estimator, are discussed in Sections IV and V. Experimental results are provided in Sections VI and VII, and conclusions are in Section VIII.

Notation: Bold upper case letters and lower case letters are used to denote matrices and column vectors, respectively. $\mathbf{I}_N$ denotes an identity matrix of size $N \times N$. $(\cdot)^T$ and $(\cdot)^H$ denote transpose and Hermitian transpose, respectively. $[\mathbf{a}]_m$ denotes the mth element of vector $\mathbf{a}$, and $[\mathbf{A}]_{m,k}$ denotes the (m,k)th element of matrix $\mathbf{A}$.

II. System Model

In this section, we present a discrete-time input-output relationship between the frequency observations at the receiver and the transmitted symbols on ZP-OFDM subcarriers, based on a path-based channel model. Such a relationship is needed for the development in Sections III–V.

A. Continuous-Time Channel Model for Block Transmissions

Assume that the data burst is divided into multiple blocks, with each block of duration $T_{\rm bl}$, and let n denote the block index. For the nth block, assume that the time-varying channel can be expressed as

$$h(t,\tau;n) = \sum_{p=1}^{N_{\rm pa}} A_p(t;n)\delta(\tau - \tau_p(t;n)), \quad t \in [0, T_{\rm bl}] \quad (1)$$

where $N_{\rm pa}$ is the number of discrete paths, $A_p(t;n)$ and $\tau_p(t;n)$ denote the amplitude and the delay of the pth path, respectively. As in [22], we adopt the following assumptions: i) within a

block, the path amplitude can be approximated using a zero-order approximation $A_p(t;n) \approx A_p[n]$, and ii) within a block, the path delay can be approximated using a first-order polynomial expansion $\tau_p(t;n) \approx \tau_p'[n] - a_p[n]t$, where $\tau_p'[n]$ is the initial delay of the nth block and $a_p[n]$ is the Doppler scale for the pth path. The channel impulse response in (1) is rewritten as

$$h(t,\tau;n) = \sum_{p=1}^{N_{\rm pa}} A_p[n]\delta(\tau - (\tau_p'[n] - a_p[n]t)), \qquad (2)$$

for $t \in [0, T_{\rm bl}]$. Let $\tilde{s}(t;n)$ denote the transmitted passband signal of the nth block. The received passband signal through the channel in (2) is

$$\tilde{y}(t;n) = \sum_{p=1}^{N_{\rm pa}} A_p[n]\tilde{s}((1+a_p[n])t - \tau_p'[n];n) + \tilde{w}(t), \quad (3)$$

for $t \in [0, T_{\rm bl}]$, where $\tilde{w}(t)$ is the ambient noise. Hence, the input-output relationship is characterized by the $N_{\rm pa}$ triplets $\{A_p[n], \tau_p'[n], a_p[n]\}$ associated with the channel.

B. Discrete-Time System Model for ZP-OFDM

We now specify $\tilde{s}(t;n)$ for ZP-OFDM. Let T denote the OFDM symbol duration and $T_{\rm g}$ the length of the guard interval between consecutive OFDM blocks, hence the OFDM block duration is $T_{\rm bl} = T + T_{\rm g}$. With the subcarrier spacing of $1/T$, a total of K subcarriers are located at frequencies

$$f_k = f_{\rm c} + k/T, \quad k = -K/2, \ldots, K/2-1 \qquad (4)$$

where $f_{\rm c}$ is the center frequency, and K is assumed even. The signal bandwidth is thus $B = K/T$.

The total number of subcarriers are divided into three non-overlapping sets $\mathcal{S}_{\rm N}, \mathcal{S}_{\rm P}, \mathcal{S}_{\rm D}$, containing null, pilot, and data subcarriers, respectively. Let $s[k;n]$ denote the symbol on the kth subcarrier of the nth block, which could be zero, a known pilot, or a data symbol. The transmitted signal of the nth OFDM block can be expressed as

$$\tilde{s}(t;n) = 2\,\mathrm{Re}\left(\sum_{k=-K/2}^{K/2-1} s[k;n]e^{j2\pi f_k t}g(t)\right), \qquad (5)$$

for $t \in [0,\ T_{\rm bl}]$, where $g(t)$ is a pulse shaping filter with the Fourier transform denoted by $G(f)$. A rectangular window $g(t)$ with nonzero support $[0,T]$ has $G(f) = \frac{\sin(\pi fT)}{\pi fT}e^{-j\pi fT}$.

As specified in [21] and [22], the following three operations are carried out on the received passband signal $\tilde{y}(t;n)$ to obtain discrete frequency-domain samples.

1) The main Doppler scaling effect of the received signal $\tilde{y}(t;n)$ is removed through the resampling operation with a resampling factor $(1+\hat{a}[n])$, leading to the resampled signal $\tilde{z}(t;n) = \tilde{y}(\frac{t}{1+\hat{a}[n]};n)$.
2) Shift the passband signal to baseband via $z(t;n) = \mathrm{LPF}(\tilde{z}(t;n)e^{-j2\pi f_{\rm c}t})$, where LPF stands for low pass filtering, and then compensate the residual Doppler effect via multiplying $z(t;n)$ by $e^{-j2\pi\hat{\epsilon}[n]t}$. (See e.g., [21] on how to obtain the Doppler scale estimate $\hat{a}[n]$ and the residual Doppler shift estimate $\hat{\epsilon}[n]$.)
3) Obtain the frequency measurement at the mth subcarrier through Fourier transform

$$z[m;n] = \frac{1}{T}\int_0^{T_{\rm bl}} z(t;n)e^{-j2\pi\hat{\epsilon}[n]t}e^{-j2\pi\frac{m}{T}t}dt. \qquad (6)$$

Following the derivation in [22], the following expression can be obtained,

$$z[m;n] = w[m;n] + \sum_{p=1}^{N_{\rm pa}}\left[\xi_p[n]e^{-j2\pi\frac{m}{T}\tau_p[n]} \times \sum_{k=-K/2}^{K/2-1} G\left(\frac{f_m+\hat{\epsilon}[n]}{1+b_p[n]} - f_k\right)s[k;n]\right] \qquad (7)$$

where $w[m;n]$ is the additive noise, and the path-specific parameters are

$$1+b_p[n] = \frac{1+a_p[n]}{1+\hat{a}[n]}, \quad \tau_p[n] = \frac{\tau_p'[n]}{1+b_p[n]},$$
$$\xi_p[n] = \frac{A_p[n]}{1+b_p[n]}e^{-j2\pi(f_{\rm c}+\hat{\epsilon}[n])\tau_p[n]}. \qquad (8)$$

Equation (7) reveals that the output measurements and the input symbols on OFDM subcarriers are uniquely related through $N_{\rm pa}$ triplets $\{\xi_p[n], \tau_p[n], b_p[n]\}$, which are equivalent complex amplitudes, delays, and Doppler scales of the propagation paths after initial processing.

For notational convenience, define two generic $K \times K$ matrices as

$$[\mathbf{\Lambda}(\tau)]_{m,m} = e^{-j2\pi\frac{m}{T}\tau},$$
$$[\mathbf{\Gamma}(b,\epsilon)]_{m,k} = G\left(\frac{f_m+\epsilon}{1+b} - f_k\right). \qquad (9)$$

Stack the frequency observations and the transmitted symbols at all subcarriers into vectors $\mathbf{z}[n]$ and $\mathbf{s}[n]$, respectively. A compact matrix-vector representation can be formulated as

$$\mathbf{z}[n] = \mathbf{H}[n]\mathbf{s}[n] + \mathbf{w}[n] \qquad (10)$$

where the noise $\mathbf{w}[n]$ is similarly defined as $\mathbf{z}[n]$, and the channel mixing matrix is

$$\mathbf{H}[n] = \sum_{p=1}^{N_{\rm pa}} \xi_p[n]\mathbf{\Lambda}(\tau_p[n])\mathbf{\Gamma}(b_p[n],\hat{\epsilon}[n]). \qquad (11)$$

Remark 1: Our derivation on the discrete-time relationship between the input symbols and the output samples prior to data detection is carried out for ZP-OFDM [22]. A similar expression is provided in [29] and [30] for cyclic-prefixed (CP)-OFDM. One can also use the channel model in (3) to derive a similar relationship for single carrier block transmissions. The proposed clustered adaptation approach in Section III is also applicable to CP-OFDM and single carrier block transmissions.

III. Cluster-Adaptation Based Block-to-Block Receiver Design

The receivers in [21] and [22] operate on a block-by-block basis, where channel estimation is performed solely based on the measurements on the pilot subcarriers of the current block. Since the pilot-based approach does not rely on channel coherence across blocks, it is robust to rapid changes across blocks, where the decoding performance of the current block is not affected by the errors in the previous block. The drawback is that a large number of pilots are needed for block-by-block channel estimation; for example, one quarter of symbols are used as pilots in [21] and [22].

We here aim to explore the channel coherence across blocks to improve the system performance relative to the existing pilot-based method. As a result, it allows the system to reduce the number of pilots while maintaining robust operation over fast-varying channels. When processing the nth block, the receiver has the previously-estimated triplets $\{\hat{\xi}_p[n-1], \hat{\tau}_p[n-1], \hat{b}_p[n-1]\}_{p=1}^{N_{\rm pa}}$ at hand, in addition to the frequency observation $\mathbf{z}[n]$ of the nth block. However, underwater acoustic channels could vary rapidly, hence the channel estimate from the preceding block should not be used directly. The following two issues need to be addressed:

1) how to model channel variations from one block to the next;
2) how to effectively combine the uncertain channel knowledge from the previous block with the noisy measurements on the pilot subcarriers from the current block.

We next present our model for channel variation, and a general description on the receiver processing module from one block to the next.

A. Clustered Block-to-Block Multipath Variation

Based on the path-based channel model [1], one may want to model the variation of each path individually. However, the effort of characterizing the variation of each path could be similar to that of directly estimating the parameters of each path. In this paper, we utilize the clustering property of channel paths, and propose a cluster-based model for channel variations across blocks.

- First, split the channel paths into $N_{\rm cl}$ clusters as

$$\{(\xi_p[n-1], \tau_p[n-1], b_p[n-1])\}_{p=1}^{N_{\rm pa}} = \bigcup_{i=1}^{N_{\rm cl}} \{(\xi_p[n-1], \tau_p[n-1], b_p[n-1])\}_{p\in\Omega_i} \quad (12)$$

  where Ω_i is a collection of paths within the ith cluster.
- Second, assume that all paths within one cluster share the same variations $\{\gamma_i, \Delta\tau_i, \Delta b_i\}$ on the complex amplitude, the delay, and the Doppler scale between adjacent blocks, however, the variations on different clusters are independent. The triplets of paths within the ith cluster of the nth block after the cluster-offset compensation are[1]

$$\begin{cases} \bar{\xi}_p[n \mid n-1] = \hat{\xi}_p[n-1] \cdot \gamma_i, \\ \bar{\tau}_p[n \mid n-1] = \hat{\tau}_p[n-1] + \Delta\tau_i, \\ \bar{b}_p[n \mid n-1] = \hat{b}_p[n-1] + \Delta b_i, \end{cases} \quad \forall\, p \in \Omega_i \quad (13)$$

  where $i = 1, \ldots, N_{\rm cl}$.

After the receiver estimates the offsets $\{\gamma_i, \Delta b_i, \Delta\tau_i\}_{i=1}^{N_{\rm cl}}$, the path parameters after cluster-offset compensation in (13) will be used to assist channel estimation of the nth block.

B. Receiver Design With Block-to-Block Channel Adaptation

The receiver incorporating the cluster-adaptation based channel estimator consists of four steps as shown in Fig. 2, with each step briefly described in the following.

- *Step 1: Cluster offset parameter estimation/compensation*. Estimate the offset parameter of each cluster based on the estimated channel $\{\hat{\xi}_p[n-1], \hat{\tau}_p[n-1], \hat{b}_p[n-1]\}_{p=1}^{N_{\rm pa}}$ from the $(n-1)$st block and the frequency observations $\mathbf{z}[n]$ of the nth block. Pass the offset-compensated channel parameters $\{\bar{\hat{\xi}}_p[n \mid n-1], \bar{\hat{\tau}}_p[n \mid n-1], \bar{\hat{b}}_p[n \mid n-1]\}$ to the hybrid sparse channel estimation.
- *Step 2: Hybrid sparse channel estimation*. Perform hybrid sparse channel estimation based on the compensated channel parameters of each cluster, the estimated cluster variances $\{\hat{\sigma}_i^2[n-1]\}_{i=1}^{N_{\rm cl}}$, and the received signal of the nth block. Pass the estimated channel matrix $\hat{\mathbf{H}}[n]$ to the symbol detection module.
- *Step 3: Symbol detection and channel decoding*. Estimate the information symbols and perform channel decoding to recover the transmitted information bits. Pass the soft estimate of information symbols $\bar{\mathbf{s}}[n]$ from the decoder to refine the channel estimate.
- *Step 4: Refined channel estimation and cluster variation estimation*. Perform the sparse channel estimation based on the estimated information symbols $\bar{\mathbf{s}}[n]$ and the measurement $\mathbf{z}[n]$ to refine the channel estimate $\{\hat{\xi}_p[n], \hat{\tau}_p[n], \hat{b}_p[n]\}_{p=1}^{N_{\rm pa}}$, and update cluster variances $\{\hat{\sigma}_i^2[n]\}_{i=1}^{N_{\rm cl}}$; both of them are passed to the next block.

In the following sections, we will provide detailed descriptions on the key receiver processing modules.

IV. Cluster Offset Estimation and Compensation

For the current block, the receiver knows the symbols on the pilot and null subcarriers. We define a $K \times K$ selector matrix $\mathbf{\Phi}$ which is a diagonal matrix with unit entry at pilot and null subcarriers, and zeros elsewhere. Define

$$\bar{\mathbf{z}}_{\rm P}[n] = \mathbf{\Phi}\mathbf{z}[n], \quad \mathbf{u}[n] = \mathbf{\Phi}\mathbf{s}[n]. \quad (14)$$

[1]Instead of $\bar{\tau}_p[n \mid n-1] = \hat{\tau}_p[n-1] + \Delta\tau_i$ in (13), we have also tried $\bar{\tau}_p[n \mid n-1] = \hat{\tau}_p[n-1] - \hat{b}_p[n-1]T_{\rm bl} + \Delta\tau_i$, where the Doppler scaling effect on the delay for each individual path is considered. However, we do not find significant performance difference between these two approaches, and hence put forward the simple expression $\bar{\tau}_p[n \mid n-1] = \hat{\tau}_p[n-1] + \Delta\tau_i$ in (13).

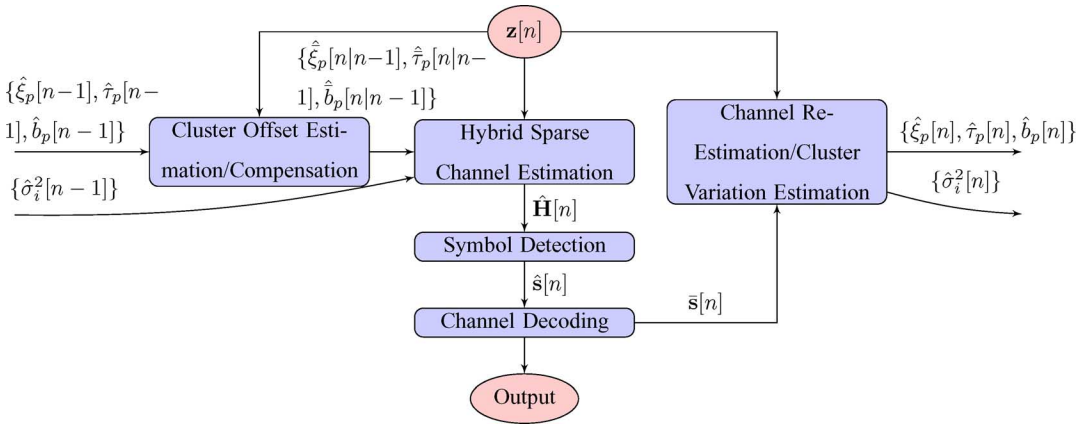

Fig. 2. Flowchart of the processing for the nth block in the proposed block-to-block receiver design.

These two vectors, known to the receiver, will be used to estimate the offset triplets $\{\gamma_i, \Delta\tau_i, \Delta b_i\}_{i=1}^{N_{\rm cl}}$.

Based on the channel variation model in (13), define the following $K \times K$ matrix $\mathbf{B}_i(\,\cdot\,)$ for the ith cluster

$$\mathbf{B}_i(\Delta\tau_i, \Delta b_i; n) = \sum_{\forall p \in \Omega_i} \hat{\xi}_p[n-1]\mathbf{\Lambda}(\bar{\tau}_p[n\,|\,n-1])\mathbf{\Gamma}(\bar{b}_p[n\,|\,n-1], \hat{\epsilon}[n]). \quad (15)$$

If the symbol vector $\mathbf{u}[n]$ is the input to an artificial channel containing only paths from the ith cluster, the frequency-domain output would be

$$\mathbf{z}_i[n] = \gamma_i \mathbf{B}_i(\Delta\tau_i, \Delta b_i; n)\mathbf{u}[n]. \quad (16)$$

Combining the contributions from all clusters, one can write

$$\bar{\mathbf{z}}_{\rm P}[n] = \sum_{i=1}^{N_{\rm cl}} \mathbf{z}_i[n] + \mathbf{v}[n] \quad (17)$$

where $\mathbf{v}(n)$ consists of the ambient noise and the error caused by the channel model mismatch. If the offset parameters for all clusters are correctly estimated, $\sum_{i=1}^{N_{\rm cl}} \mathbf{z}_i[n]$ would match $\bar{\mathbf{z}}_{\rm P}[n]$ closely. Hence, offset parameters can be estimated via the following optimization problem:

$$\min_{\{\gamma_i, \Delta\tau_i, \Delta b_i\}_{i=1}^{N_{\rm cl}}} \left\| \bar{\mathbf{z}}_{\rm P}[n] - \sum_{i=1}^{N_{\rm cl}} \gamma_i \mathbf{B}_i(\Delta\tau_i, \Delta b_i; n)\mathbf{u}[n] \right\|_2^2. \quad (18)$$

Once the offset triplets $\{\hat{\gamma}_i, \Delta\hat{\tau}_i, \Delta\hat{b}_i\}_{i=1}^{N_{\rm cl}}$ are estimated, the estimates of channel parameters $\{\hat{\bar{\xi}}_p[n\,|\,n-1], \hat{\bar{\tau}}_p[n\,|\,n-1], \hat{\bar{b}}_p[n\,|\,n-1]\}$ are passed to the channel estimation module.

A. Exhaustive Search

The tentative measurement vector $\mathbf{z}_i[n]$ in (16) is linear in γ_i, but nonlinear with respect to $\Delta\tau_i$ and Δb_i. Note that for each setting of $\{\Delta\tau_i, \Delta b_i\}_{i=1}^{N_{\rm cl}}$, the complex amplitudes $\{\gamma_i\}_{i=1}^{N_{\rm cl}}$ can be easily obtained via the least-squares approach. Hence, a brute force method is to try all the possible values $\{\Delta b_i, \Delta\tau_i\}_{i=1}^{N_{\rm cl}}$ and choose the optimal one.

Specifically, let us define a two-dimensional grid where $\{\Delta b_i, \Delta\tau_i\}$ falls on

$$\Delta\tau_i \in \{-\Delta\tau_{\max}, \Delta\tau_{\max} + \delta_\tau, \ldots, \Delta\tau_{\max}\} \quad (19)$$

$$\Delta b_i \in \{-\Delta b_{\max}, -\Delta b_{\max} + \delta_b, \ldots, \Delta b_{\max}\} \quad (20)$$

for $i = 1, \ldots, N_{\rm cl}$, where δ_τ and δ_b are the step size in the two-dimensional delay and Doppler plane. Although here we assume that all clusters share a common set of representative offset values, extension to the scenario defining different representative sets for different clusters is straightforward, and will not be pursued here.

Assume that there are N_1 grid points on the delay dimension, and N_2 grid points on the Doppler scale dimension. The exhaustive search has a complexity proportional to $(N_1 N_2)^{N_{\rm cl}}$, which becomes prohibitive when the number of clusters is large.

B. Orthogonal Matching Pursuit

A suboptimal greedy algorithm, orthogonal matching pursuit (OMP) [31], can be used to solve (18) at low computational complexity. On the delay-Doppler plane as defined in (19) and (20), let $\gamma_{i,l,j}$ denote the complex amplitude corresponding to the grid point $(\Delta\tau[l], \Delta b[j])$ for the ith cluster. The frequency observation vector $\bar{\mathbf{z}}_{\rm P}[n]$ can be formulated as

$$\bar{\mathbf{z}}_{\rm P}[n] = \sum_{i=1}^{N_{\rm cl}} \sum_{l=1}^{N_1} \sum_{j=1}^{N_2} \gamma_{i,j,l} \mathbf{B}_i(\Delta\tau[l], \Delta b[j]; n)\mathbf{u}[n] + \mathbf{v}[n]. \quad (21)$$

Defining vectors of size $K \times 1$ as

$$\mathbf{p}_{i,j,l} = \mathbf{B}_i(\Delta\tau[l], \Delta b[j]; n)\mathbf{u}[n], \quad (22)$$

we can rewrite (21) as

$$\bar{\mathbf{z}}_{\rm P}[n] = [\,\mathbf{p}_{1,1,1}, \ldots, \mathbf{p}_{N_{\rm cl},N_1,N_2}\,] \begin{pmatrix} \gamma_{1,1,1} \\ \vdots \\ \gamma_{N_{\rm cl},N_1,N_2} \end{pmatrix} + \mathbf{v}[n]. \quad (23)$$

When using the OMP algorithm to find $\hat{\gamma}_{i,l,j}$, we will enforce that *there is only one delay and Doppler offset pair with nonzero amplitude for each cluster*. Hence, the OMP algorithm will stop after $N_{\rm cl}$ steps, and its complexity is linear in the number of clusters.

C. An Important Special Case With Only Amplitude and Delay Variations

We now consider an important special case with only amplitude and delay variations

$$\begin{cases} \bar{\xi}_p[n \,|\, n-1] = \hat{\xi}_p[n-1] \cdot \gamma_i, \\ \bar{\tau}_p[n \,|\, n-1] = \hat{\tau}_p[n-1] + \Delta\tau_i \end{cases} \quad \forall\, p \in \Omega_i. \tag{24}$$

In other words, the Doppler scale variation in (13) is set to be $\Delta b_i = 0$. This way, we have (25), shown at the bottom of the page. The vector $\hat{\mathbf{p}}_i[n]$ can be precomputed. The optimization problem in (18) is now simplified to

$$\min_{\{\gamma_i, \Delta\tau_i,\}_{i=1}^{N_{\rm cl}}} \left\| \bar{\mathbf{z}}_{\rm P}[n] - \sum_{i=1}^{N_{\rm cl}} \gamma_i \mathbf{\Lambda}(\Delta\tau_i) \hat{\mathbf{p}}_i[n] \right\|_2^2. \tag{26}$$

Similarly, the optimization problem can be solved by exhaustive search and the OMP algorithm. The exhaustive search along the delay grid in (19) has a complexity $N_1^{N_{\rm cl}}$. The OMP algorithm still needs $N_{\rm cl}$ steps, however, within each step, there are much less templates to correlate. This special case with $\Delta b_i = 0$ hence has a major complexity advantage relative to the general case with $\Delta b_i \neq 0$.

V. Cluster-Adaptation Based Sparse Channel Estimation

In this section, we develop a sparse channel estimator that incorporates the inputs from both the $(n-1)$st and nth blocks. Other receiver modules in Fig. 2 following channel estimation will be also briefly discussed.

A. Hybrid Sparse Channel Estimation

The resources available for channel estimation on the nth block include: i) the offset-compensated triplets $\{\hat{\bar{\xi}}_p[n \,|\, n-1], \hat{\bar{\tau}}_p[n \,|\, n-1], \hat{\bar{b}}_p[n \,|\, n-1]\}$, and ii) the frequency observation vector $\bar{\mathbf{z}}_{\rm P}[n]$ and the corresponding symbol vector $\mathbf{u}[n]$.

To utilize the $\{(\hat{\bar{\xi}}_p[n \,|\, n-1], \hat{\bar{\tau}}_p[n \,|\, n-1], \hat{\bar{b}}_p[n \,|\, n-1]), \forall p \in \Omega_i\}_{i=1}^{N_{\rm cl}}$ in a way similar to the pilot-based channel estimation approach, we will construct a set of artificial measurements $\{\breve{\mathbf{z}}_i[n]\}_{i=1}^{N_{\rm cl}}$ by passing a known symbol vector $\breve{\mathbf{s}}[n]$ through $N_{\rm cl}$ channels formed by paths from $N_{\rm cl}$ clusters, respectively. The transmitted symbol vector $\breve{\mathbf{s}}(n)$ is arbitrary but known, and is often constructed by drawing each symbol from a QPSK constellation. Similar to (11), let us define the following two channel matrices corresponding to the ith cluster as

$$\hat{\bar{\mathbf{H}}}_i[n \,|\, n-1] = \sum_{\forall p \in \Omega_i} \hat{\bar{\xi}}_p[n \,|\, n-1] \times \mathbf{\Lambda}(\hat{\bar{\tau}}_p[n \,|\, n-1]) \mathbf{\Gamma}(\hat{\bar{b}}_p[n \,|\, n-1], \hat{\epsilon}[n]) \tag{27}$$

$$\mathbf{H}_i[n] = \sum_{\forall p \in \Omega_i} \xi_p[n] \mathbf{\Lambda}(\tau_p[n]) \mathbf{\Gamma}(b_p[n], \hat{\epsilon}[n]). \tag{28}$$

The artificial measurements are constructed as

$$\begin{aligned} \breve{\mathbf{z}}_i[n] &= \hat{\bar{\mathbf{H}}}_i[n \,|\, n-1] \breve{\mathbf{s}}(n) \\ &= \mathbf{H}_i[n] \breve{\mathbf{s}}[n] + \underbrace{(\hat{\bar{\mathbf{H}}}_i[n \,|\, n-1] - \mathbf{H}_i[n]) \breve{\mathbf{s}}[n]}_{:= \breve{\mathbf{w}}_i[n]} \end{aligned} \tag{29}$$

where $\breve{\mathbf{w}}_i(n)$ denotes the residual error.

The receiver thus has measurements from different sources

$$\begin{cases} \bar{\mathbf{z}}_{\rm P}[n] = \mathbf{H}[n] \mathbf{u}[n] + \mathbf{w}[n], \\ \breve{\mathbf{z}}_i[n] = \mathbf{H}_i[n] \breve{\mathbf{s}}[n] + \breve{\mathbf{w}}_i[n], \qquad i = 1, \ldots, N_{\rm cl}. \end{cases} \tag{30}$$

These measurements have different reliabilities. We will assume that $\mathbf{w}[n]$ can be approximated by a zero-mean Gaussian noise vector with covariance matrix $\hat{\sigma}_0^2[n] \mathbf{I}_K$, and $\breve{\mathbf{w}}_i[n]$ by a zero-mean Gaussian vector with covariance matrix $\hat{\sigma}_i^2[n-1] \mathbf{I}_K$. The noise variance $\sigma_o^2[n]$ can be estimated based on frequency measurements at null subcarriers

$$\hat{\sigma}_o^2[n] = \mathbb{E}\left[|z[m;n]|^2\right], \quad \forall m \in \mathcal{S}_{\rm N}. \tag{31}$$

The estimates of $\sigma_i^2[n-1], i = 1, \ldots, N_{\rm cl}$, are passed from the previous block; the estimation procedure will be described in Section V-C.

To exploit the sparsity of channel paths, we define a set formed by all the possible values of the path delay and Doppler scale [22]

$$\tau \in \{0, T/(\beta K), 2T/(\beta K), \ldots, T_g\}_{1 \times N_\tau} \tag{32}$$

$$b \in \{-b_{\max}, -b_{\max} + \Delta b, \ldots, b_{\max}\}_{1 \times N_D} \tag{33}$$

where $T/(\beta K)$ and Δb are the uniform sampling steps on the delay and the Doppler scale, respectively, and β is the delay domain oversampling factor. Define $\xi_{j,l}$ as the complex amplitude of the path at the (τ_l, b_j) grid. For notational convenience, define

$$\begin{aligned} \mathbf{a}_{j,l} &= \mathbf{\Lambda}(\tau_l) \mathbf{\Gamma}(b_j, \hat{\epsilon}[n]) \mathbf{u}[n] \\ \mathbf{b}_{j,l} &= \mathbf{\Lambda}(\tau_l) \mathbf{\Gamma}(b_j, \hat{\epsilon}[n]) \breve{\mathbf{s}}[n]. \end{aligned} \tag{34}$$

$$\begin{aligned} \mathbf{B}_i(\Delta\tau_i, 0; n) \mathbf{u}[n] &= \sum_{\forall p \in \Omega_i} \hat{\xi}_p[n-1] \mathbf{\Lambda}(\bar{\tau}_p[n \,|\, n-1]) \mathbf{\Gamma}(\hat{b}_p[n-1], \hat{\epsilon}[n]) \mathbf{u}[n] \\ &= \mathbf{\Lambda}(\Delta\tau_i) \underbrace{\sum_{\forall p \in \Omega_i} \hat{\xi}_p[n-1] \mathbf{\Lambda}(\hat{\tau}_p[n-1]) \mathbf{\Gamma}(\hat{b}_p[n-1], \hat{\epsilon}[n]) \mathbf{u}[n]}_{:= \hat{\mathbf{p}}_i[n]}. \end{aligned} \tag{25}$$

The frequency measurements of the current block can be expressed as

$$\begin{aligned}\bar{\mathbf{z}}_{\mathrm{P}}[n] &= \sum_{j=1}^{N_D}\sum_{l=1}^{N_\tau}\xi_{j,l}\mathbf{a}_{j,l} + \mathbf{w}[n] \\ &= \underbrace{[\,\mathbf{a}_{1,1},\ldots,\mathbf{a}_{N_D,N_\tau}\,]}_{:=\mathbf{A}}\underbrace{\begin{pmatrix}\xi_{1,1}\\ \vdots \\ \xi_{N_D,N_\tau}\end{pmatrix}}_{:=\boldsymbol{\xi}} + \mathbf{w}(n) \\ &= \mathbf{A}\boldsymbol{\xi} + \mathbf{w}[n]. \end{aligned} \tag{35}$$

Define $\boldsymbol{\Theta}_i$ as a selector of channel paths within the ith cluster, being a diagonal matrix of size $N_D N_\tau \times N_D N_\tau$, and with unit entry for grids within a zone where the paths of the ith cluster can reside, and zeros elsewhere (See Figs. 6 and 8 for the plots on the zones for different clusters). Similar to (35), define

$$\mathbf{B} = [\,\mathbf{b}_{1,1},\ldots,\mathbf{b}_{N_D,N_\tau}\,] \tag{36}$$

which leads to a similar expression for the artificial measurements

$$\breve{\mathbf{z}}_i[n] = \mathbf{B}\boldsymbol{\Theta}_i\boldsymbol{\xi} + \breve{\mathbf{w}}[n]. \tag{37}$$

We are now ready to present two sparse channel estimators, where one does not enforce the paths for the nth block to fall into the specified zones for all clusters and one does. For the former case, the solution is obtained as

$$\begin{aligned}\hat{\boldsymbol{\xi}} = \arg\min_{\boldsymbol{\xi}}\ & \frac{1}{\hat{\sigma}_0^2[n]}\|\bar{\mathbf{z}}_{\mathrm{P}}[n] - \mathbf{A}\boldsymbol{\xi}\|^2 \\ & + \sum_{i=1}^{N_{\mathrm{cl}}}\frac{1}{\hat{\sigma}_i^2[n-1]}\|\breve{\mathbf{z}}_i[n] - \mathbf{B}\boldsymbol{\Theta}_i\boldsymbol{\xi}\|^2 + \zeta\|\boldsymbol{\xi}\|_1 \end{aligned} \tag{38}$$

where $|\boldsymbol{\xi}|_1$ denotes the ℓ_1 norm of vector $\boldsymbol{\xi}$, and ζ controls the sparsity of the solution. For the latter case, the solution is obtained as

$$\begin{aligned}\hat{\boldsymbol{\xi}} = \arg\min_{\boldsymbol{\xi}}\ & \frac{1}{\hat{\sigma}_0^2[n]}\left\|\bar{\mathbf{z}}_{\mathrm{P}}[n] - \mathbf{A}\sum_{i=1}^{N_{\mathrm{cl}}}\boldsymbol{\Theta}_i\boldsymbol{\xi}\right\|^2 \\ & + \sum_{i=1}^{N_{\mathrm{cl}}}\frac{1}{\hat{\sigma}_i^2[n-1]}\|\breve{\mathbf{z}}_i[n] - \mathbf{B}\boldsymbol{\Theta}_i\boldsymbol{\xi}\|^2 + \zeta\|\boldsymbol{\xi}\|_1. \end{aligned} \tag{39}$$

Clearly, in the solution of (39), the entries outside the specified zones of N_{cl} clusters are zero. Compressive sensing [32] techniques can be used to solve these regularized least-squares problems, and we use the SpaRSA algorithm from [33] in this paper. Once $\hat{\boldsymbol{\xi}}$ is obtained, $\hat{\mathbf{H}}[n]$ can be computed from (11), which will be used for symbol detection.

B. Symbol Detection and Channel Decoding

Symbol detection can be performed according to the maximum *a posterior* (MAP) or the minimum mean square error (MMSE) criteria. In this paper, we adopt a linear MMSE equalizer

$$\hat{\mathbf{s}}[n] = \left[\hat{\mathbf{H}}[n]^H\hat{\mathbf{H}}[n] + \hat{\sigma}_o^2[n]\mathbf{I}_K\right]^{-1}\hat{\mathbf{H}}[n]^H\mathbf{z}[n]. \tag{40}$$

For practical implementation, a banded structure will be imposed on the channel matrix $\hat{\mathbf{H}}[n]$; see more discussion in Section VI. This way, low-cost MMSE equalization can be achieved, through, e.g., a factor-graph based filtering approach [34].

After inputting the LMMSE estimate of information symbols to a channel decoder the *a posterior* probabilities (APP) of information symbols can be obtained as the decoder output, which are then used to calculate both soft and hard estimates of information symbols [35]. In this paper, the soft decisions of information symbols are used to refine the channel estimate.

C. Channel Re-Estimation and Cluster Variance Update

Based on the supplied symbols from the decoder denoted as $\bar{\mathbf{s}}[n]$, we have the input-output relationship as $\mathbf{z}[n] = \mathbf{H}[n]\bar{\mathbf{s}}[n] + \mathbf{v}[n]$, where all the measurements in $\mathbf{z}[n]$ of the current block are used for channel estimation. This is a straightforward extension of the block-by-block sparse channel estimator in [22]. The refined estimates on the path parameters are passed to the next block.

Based on the updated channel estimate $\hat{\boldsymbol{\xi}}$, the variance of artificial measurements corresponding to the ith cluster can be updated as

$$\hat{\sigma}_i^2[n] = \frac{1}{K}\|\breve{\mathbf{z}}_i[n] - \mathbf{B}\boldsymbol{\Theta}_i\hat{\boldsymbol{\xi}}\|^2 \tag{41}$$

The variance $\hat{\sigma}_i^2[n]$ will be used for the hybrid channel estimation of the $(n+1)$st block. Note that one can also filter the measurements by $\hat{\sigma}_i^2[n] = \nu\hat{\sigma}_i^2[n-1] + (1-\nu)\|\breve{\mathbf{z}}_i[n] - \mathbf{B}\boldsymbol{\Theta}_i\hat{\boldsymbol{\xi}}\|^2/K$, where the forgetting factor ν can be tuned.

VI. Experimental Results: MACE10

The *mobile acoustic communication experiment* (MACE10) was carried out off the coast of Martha's Vineyard, MA, June 2010. The water depth was about 80 m. The receiving array was stationary, while the source was towed slowly away from the receiver and then towed back, at a speed around 1 m/s. The relative distance of the transmitter and the receiver changed from 500 to 4.5 km. Out of two tows in the experiment, we only consider the data collected in the first tow. There are 31 transmissions in this tow, with 20 blocks in each transmission. We exclude one transmission file recorded during the turn of the source, where the signal-to-noise-ratio (SNR) of the received signal is quite low.

Parameters of this experiment are summarized in Table I. Out of 1024 subcarriers, there are $|\mathcal{S}_N| = 96$ null subcarriers with 24 on each edge of the signal band for band protection and 48 evenly distributed in the middle for the carrier frequency offset estimation; there are $|\mathcal{S}_{\mathrm{P}}| = 256$ pilot subcarriers uniformly distributed among the 1024 subcarriers, and the remaining are $|\mathcal{S}_{\mathrm{D}}| = 672$ data subcarriers for delivering information symbols. A rate-1/2 nonbinary LDPC code is used, where the size of the Galois field matches the size of the constellation [35].

Despite having 256 pilots in our signal design, we only use part of them to investigate performance of the proposed channel estimator. Define $|\mathcal{S}'_{\mathrm{P}}|$ as the number of pilots used for channel

TABLE I
OFDM PARAMETERS IN THE MACE10 EXPERIMENT

center frequency:	f_c	13 kHz
bandwidth:	B	4.883 kHz
# of subcarriers:	K	1024
time duration:	T	209.7 ms
frequency spacing:	$\Delta f \triangleq 1/T$	4.77 Hz
guard interval:	T_g	40.3 ms

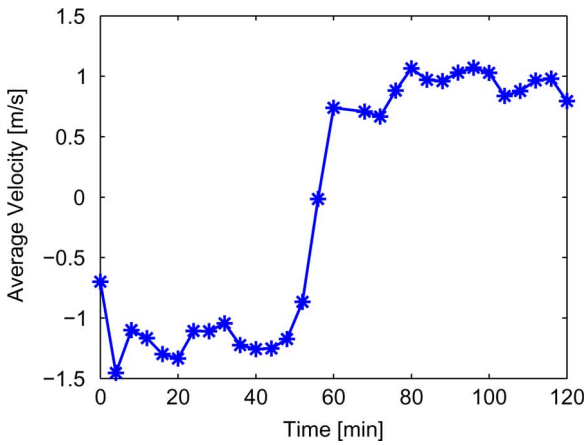

Fig. 3. Estimated average velocity using a CP-OFDM preamble, Tow 1.

estimation. For a constellation size M, the spectral efficiency and the data rate are formulated as

$$\alpha = \frac{T}{T+T_g}\cdot\frac{|\mathcal{S}_{\rm D}|}{|\mathcal{S}_D|+|\mathcal{S}'_P|+|\mathcal{S}_N|}\frac{1}{2}\cdot\log_2 M \text{ b/s/Hz} \quad (42)$$

$$R = \alpha B \text{ b/s}. \quad (43)$$

Hence, if we had used $|\mathcal{S}'_P| = 64$ pilots rather than 256 pilots in the signal design, both spectral efficiency and data rate would be increased by 23%.

To remove the Doppler effect caused by the mobility of the source array, an overall resampling operation is performed for each transmission. The overall resampling factor is estimated based on a CP-OFDM preamble prior to each transmission [36]. The estimated velocity of the source array over the first tow is shown in Fig. 3.

For multipath clustering, we have tried several algorithms, as follows.

- From a cluster detection point of view, a Page-test along the delay axis, can be used to determine the starting and ending points of the delay of each cluster at each possible Doppler rate value [37].
- From a clustering point of view, the traditional k-means algorithm [38] can be employed after a thresholding operation to eliminate noise samples in the channel estimate.
- In scenarios with a stable clustering structure, cluster locations can also be taken as priors.

Based on our experience, there is not much difference of the three strategies in terms of receiver decoding performance. In this paper, we assume that the clustering structure does not change within each transmission, and adopt the Page-test for clustering based on the channel estimate of the preamble.

For practical receiver implementation, we adopt a limited ICI-span assumption that

$$[\hat{\mathbf{H}}[n]]_{m,k} = 0, \quad \forall |m-k| > D. \quad (44)$$

This assumption is enforced in two receiver modules: i) sparse channel estimation as in (38) or (39), and ii) MMSE equalization as in (40). When $D = 0$, ICI is ignored and the receiver is termed as "ICI-ignorant" [21]. When $D > 0$, ICI is explicitly accounted for and the receiver is termed as "ICI-aware" [22].

Throughout the experimental decoding in this paper, the step size for the delay offset estimation in (19) is $\delta_\tau = 1/(2B)$ with the maximum delay offset $\Delta\tau_{\max} = 8\delta_\tau$, and the step size for the Doppler offset estimation in (20) is $\delta_b = \Delta b_{\max}/7$, where the maximum Doppler offset is set as $\Delta b_{\max} = 5\times 10^{-4}$, which corresponds to a maximum speed offset $\Delta v_{\max} = \Delta b_{\max} c = 0.75$ m/s where $c = 1500$ m/s is the sound speed in water.[2] Hence, the numbers of searching grids on the delay and Doppler domains are $N_1 = 17$ and $N_2 = 15$, respectively. For the sparse channel estimation, the delay domain oversampling factor in (32) is set as $\beta = 2$, and the maximum Doppler scale for the ICI-aware receiver is taken as $b_{\max} = 5\times 10^{-4}$ with a step size $\Delta b = b_{\max}/7$.

A. BLER Performance With Overall Resampling

To investigate the performance of the proposed channel estimator, we use $|\mathcal{S}'_P| = 32$ pilots for channel estimation and introduce 24 data subcarriers as extra pilots to estimate the Doppler scale offset, which leads to a spectral efficiency and a data rate

$$\alpha = \frac{T}{T+T_g}\cdot\frac{336-24}{672+32+96}\log_2 16 = 1.31 \text{ b/s/Hz} \quad (45)$$

$$R = \alpha B = 6.39 \text{ kb/s}. \quad (46)$$

For the MACE10 data, we use the ICI-ignorant receiver with $D = 0$. By treating all paths as in one cluster, the block-error-rate (BLER) performance of the receiver corresponding to several channel estimation schemes is shown in Fig. 4, with the setting of each scheme listed in the following:

1) "pilot-based method": the block-by-block pilot based channel estimator [22];
2) "proposed method without offset compensation": the channel is assumed stationary over blocks, setting $\Delta\tau = 0, \Delta b = 0$, and $\gamma = 1$; the hybrid channel estimation is performed without using the zone information of clusters;
3) "proposed method, $\Delta b = 0$, without zone information": the channel variation is only modeled with the delay and amplitude offsets, and set $\Delta b = 0$; the hybrid channel estimation is performed without using the zone information of clusters;
4) "proposed method, $\Delta b = 0$, with zone information": the channel variation is only modeled with the delay and amplitude offsets, and set $\Delta b = 0$; the hybrid channel estimation is performed with the zone information of clusters;

[2]The two-dimensional search window size, i.e., the maximum delay and Doppler offsets, depends on the channel variation across blocks. Typically, one can refer the variability of estimated channels in preceding blocks to decide a reasonable search window size. On the other hand, the search step sizes can be decided based on the tradeoff between the decoding performance and the computational complexity.

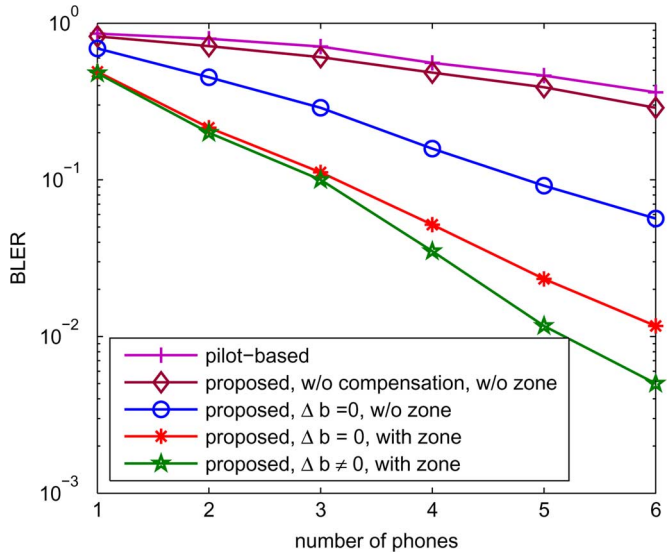

Fig. 4. BLER performance of the ICI-ignorant receiver, 16-QAM, with an overall resampling. All the channel paths are treated as in one cluster.

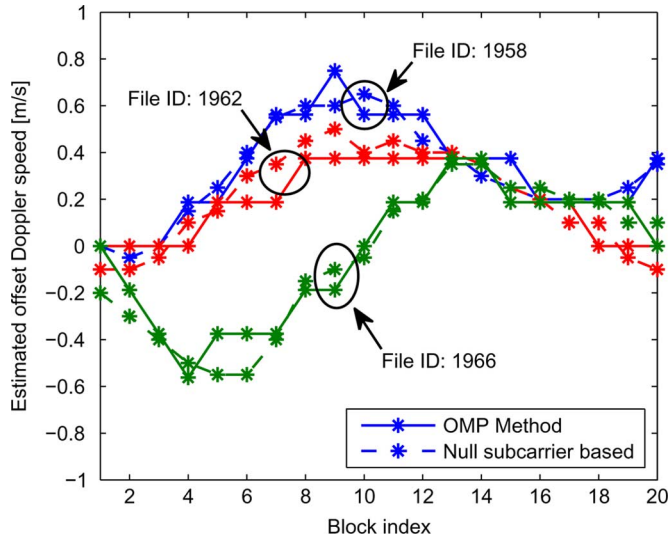

Fig. 5. Samples of estimated offset Doppler speed over 20 OFDM blocks after an overall resampling operation. All the channel paths are treated as in one cluster.

5) "proposed method, $\Delta b \neq 0$, with zone information": the channel variation is modeled with the delay, amplitude and Doppler scale offsets. The hybrid channel estimation is performed with the zone information of clusters.

We have the following observations from Fig. 4: i) exploiting the time-coherence of UWA channels boosts the decoding performance significantly, as can be seen from the performance of the pilot-based method and that of schemes corresponding to the proposed method; ii) compensation of channel variation over blocks is necessary, as can be seen from the performance of the proposed method without the offset compensation and that of the methods with the offset compensation; iii) utilizing the zone information is beneficial, as can be seen from the performance of the proposed method without zone information and that of the methods with the zone information; iv) introducing the Doppler scale offset improves the decoding performance, as can be seen from the performance of the proposed method with $\Delta b = 0$ and that with $\Delta b \neq 0$.

Fig. 5 shows the estimated Doppler speed of each block, i.e., the accumulation of Δb estimates up to the nth block, using the proposed offset-estimation method. One can find that the estimate matches well with the Doppler speed estimate using the null-subcarrier based method [21], [39]. Hence, even after an overall resampling operation performed on each data burst, the residual Doppler scaling effect within each block is not negligible. The proposed method is able to estimate the Doppler scale variation across blocks, which leads to performance improvement.

B. BLER Performance With Refined Resampling

In this subsection, we investigate the performance of the proposed channel estimator after a refined resampling operation on each individual block. The resampling factor in each block is estimated using the null-subcarrier based method [21], [39]. As shown in Fig. 6, the paths after the refined resampling are quite centered around the zero Doppler scale. We hence assume $\Delta b_i = 0$ and test the performance of the proposed channel estimator using different numbers of clusters.

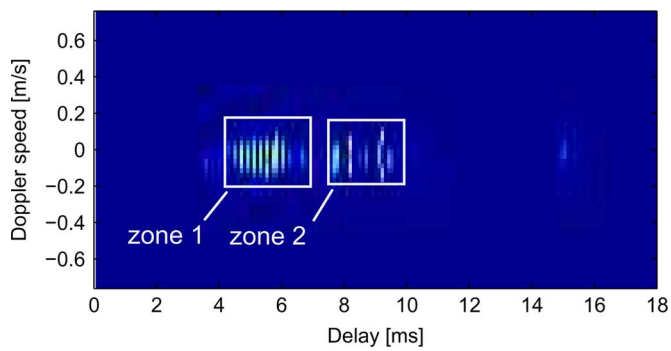

Fig. 6. MACE10: Sample of channel estimates with an OFDM preamble. A Page-test based clustering algorithm is used.

To compare the channel estimation performance with different number of clusters, we test two clustering schemes: i) treating the whole channel as single cluster; and ii) dividing channel paths into two clusters as shown in Fig. 6. We use $|\mathcal{S}'_P| = 64$ pilots for channel estimation, which leads to a spectral efficiency $\alpha = 1.36$ b/s/Hz and a data rate $R = 6.62$ kb/s.

The decoding performance of several channel estimation schemes is shown in Fig. 7. One can see a significant performance gap between the block-by-block channel estimator and the proposed channel estimators. Moreover, utilizing the zone information and treating the multipath clusters individually bring considerable performance improvement. Although paths in the second zone in Fig. 6 can be further divided into different clusters, the decoding performance with more than two clusters has been found almost identical to that with two clusters.

VII. Experimental Results: SPACE08

The *surface processes and acoustic communications experiment* (SPACE08) was held off the coast of Martha's Vineyard, Massachusetts, from Oct. 14 to Nov. 1, 2008. The water depth was about 15 meters. Among all the six receivers, we only consider the data collected by the receiver labeled as S1 which was 60 m away from the transmitter due to its interesting clustered

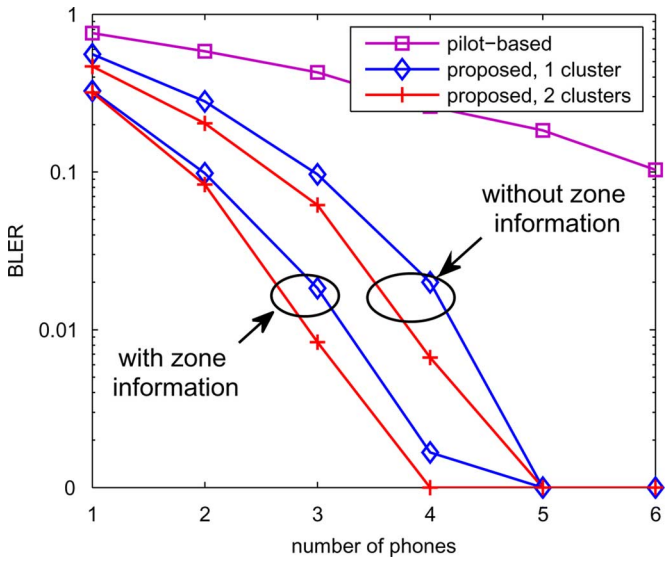

Fig. 7. BLER performance of the ICI-ignorant receiver with different number of phones combined, 16-QAM, with refined resampling for each block, 64 pilots. The curves marked with "without zone information" correspond to the formulation in (38), and those marked with "with zone information" correspond to the formulation in (39).

TABLE II
OFDM PARAMETERS IN THE SPACE08 EXPERIMENT

center frequency:	f_c	13 kHz
bandwidth:	B	9.77 kHz
# of subcarriers:	K	1024
time duration:	T	104.86 ms
frequency spacing:	$\Delta f \triangleq 1/T$	9.54 Hz
guard interval:	T_g	24.6 ms

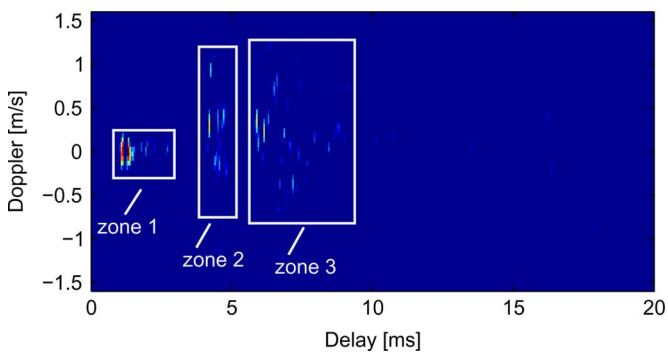

Fig. 8. SPACE08: Sample of channel estimates with an OFDM preamble. Paths in the first zone correspond to direct transmission, while paths in the second and the third zones correspond to the surface/bottom reflections. A Page-test based clustering algorithm is used.

channel structure. During the experiment, there are two periods, one around Julian date 297 and the other around Julian date 300, when the wave height and wind speed were larger than those in the rest of days [22]. The later period was more severe. For each day, there are ten recorded files, each consisting of twenty OFDM blocks. However, some data files recorded in the afternoon on Julian data 300 were distorted, which are excluded for the performance test.

Parameter settings of this experiment are summarized in Table II. Distribution of 1024 subcarriers is identical to that

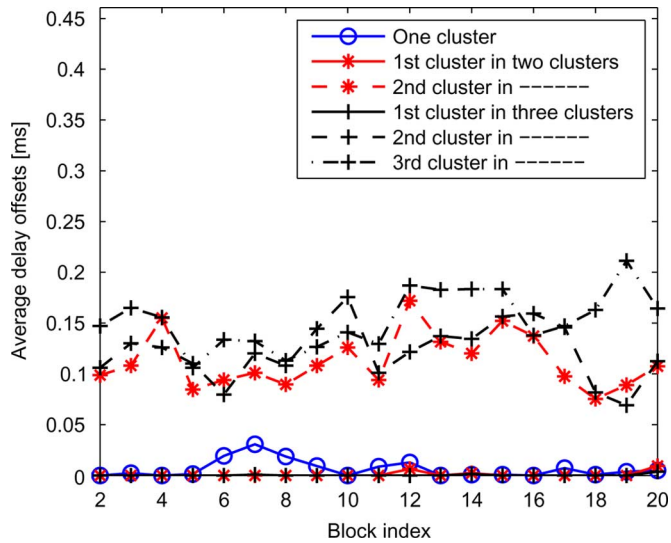

Fig. 9. The absolute values of the estimated delay offsets for different settings for one data burst of 20 blocks.

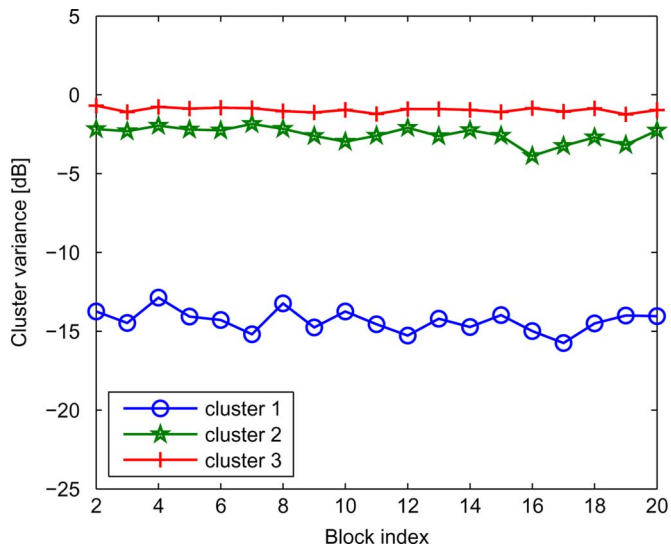

Fig. 10. Estimated variances of three clusters normalized by the power of each cluster, averaged over 12 phones of data files collected in Julian date 297.

in the MACE10 experiment. Again, we only consider part of pilot subcarriers for channel estimation. Formulation of the data rate is identical to (42). For the SPACE08 data, we use an ICI-aware receiver with $D = 1$. To perform the ICI-aware channel estimation in the time-varying scenario, we introduce 24 data subcarriers as extra pilots for the ICI coefficients estimation, leading to a spectral efficiency $\alpha = 1.22$ b/s/Hz and a data rate $R = 11.9$ kb/s for $|\mathcal{S}'_{\mathrm{P}}| = 64$.

During the experiment, since both transmitter and receiver were stationary, no resampling operation is applied to the received signal, and we assume that there is no Doppler scale offset over consecutive blocks, i.e., $\{\Delta b_i = 0\}$ for all clusters. The maximum delay offset and grid size are identical to the values described in Section VI, so as the parameter values for the hybrid channel estimation.

Sample of one particular estimated channel impulse response is demonstrated in Fig. 8, where channel paths are grouped into

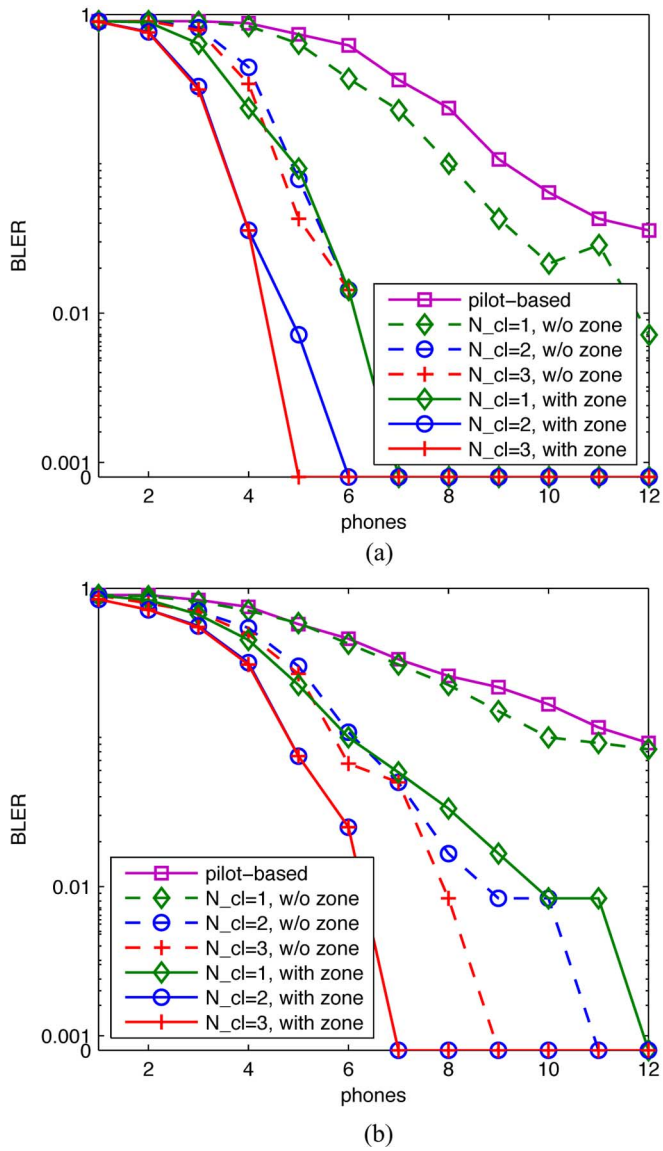

Fig. 11. BLER performance of the ICI-aware receiver ($D = 1$) with different channel estimation schemes, 16-QAM. N_{cl}: the number of clusters. (a) Julian Date: 297 and (b) Julian Date: 300.

three clusters: the first cluster corresponds to direct transmissions, the second and the third clusters correspond to the surface and bottom reflections, respectively.

As can be seen from Fig. 1, paths formed by the direct transmissions are quite stable, while the paths constituted by the reflected paths tend to scatter around with a very large fluctuation. To compare the channel estimation performance with different number of clusters, we test three clustering schemes, i) treating all the paths as in one single cluster; ii) dividing channel paths into two clusters, i.e., one cluster formed by refractions and the other cluster formed by reflections; and iii) dividing channel paths into three clusters, i.e., one cluster by refractions and two clusters by reflections, respectively, as shown in Fig. 8.

Fig. 9 shows the estimated delay offset for different settings for one file collected in Julian date 297. Fig. 10 shows the estimated variances of three clusters normalized by the power of each cluster averaged over twelve phones of data files collected in Julian date 297. Both plots confirm that the first cluster is much more stable than the other two clusters, hence it is advantageous to model different variations for different clusters.

Fig. 11 demonstrates the averaged BLER performance of files collected in Julian date 297 and Julian date 300 using the proposed channel estimator and the pilot-based block-by-block channel estimator. One can find that the proposed block-to-block receiver outperforms the pilot-based block-by-block receiver considerably. By modeling the variations of multipath clusters independently and utilizing the cluster support information for hybrid channel estimation, the system performance has been significantly improved.

VIII. Conclusion

Inspired by the fact that the propagation paths in UWA channels tend to be clustered, and each cluster varies independently, we proposed a channel variation model where paths within each cluster share common amplitude, delay, and Doppler scale offsets across consecutive blocks. Based on the availability of pilot tones in the OFDM transmission, we developed a method to estimate the offset parameters, and a hybrid channel estimator was then proposed to combine the offset-compensated channel estimate from the previous block with the pilot observations of the current block, in which both the zone information and variances of clusters were incorporated.

Data sets collected from two experiments were used to validate the performance of the proposed method. Using a moderate number of pilot subcarriers, say 64 instead of 256 available pilot subcarriers, the proposed cluster-adaptation based method with two or three clusters and the cluster-zone information can reduce by half the number of receiving elements needed relative to the pilot-based channel estimator, for a satisfactory performance of block error rate around 10^{-2}.

Acknowledgment

The authors would like to thank L. Freitag and his team for conducting the MACE10 experiment.

References

[1] Z.-H. Wang, S. Zhou, J. Preisig, K. Pattipati, and P. Willett, "Per-cluster-prediction based sparse channel estimation for multicarrier underwater acoustic communications," in *Proc. IEEE Int. Conf. Signal Process., Commun., Comput.*, Xi'an, China, Sep. 2011.

[2] D. B. Kilfoyle and A. B. Baggeroer, "The state of the art in underwater acoustic telemetry," *IEEE J. Ocean. Eng.*, vol. 25, no. 1, pp. 4–27, Jan. 2000.

[3] M. Stojanovic and J. Preisig, "Underwater acoustic communication channels: Propagation models and statistical characterization," *IEEE Commun. Mag.*, vol. 47, no. 1, pp. 84–89, Jan. 2009.

[4] T. C. Yang, "Characteristics of underwater acoustic communication channels in shallow water," in *Proc. MTS/IEEE OCEANS Conf.*, Santander, Spain, Jun. 2011.

[5] X. Geng and A. Zielinski, "An eigenpath underwater acoustic communication channel model," in *Proc. MTS/IEEE OCEANS Conf.*, San Diego, CA, Oct. 1995, pp. 1189–1196.

[6] M. Badiey, Y. Mu, J. Simmen, and S. Forsythe, "Signal variability in shallow-water sound channels," *IEEE J. Ocean. Eng.*, vol. 25, no. 4, pp. 492–500, Oct. 2000.

[7] J. C. Preisig and G. B. Deane, "Surface wave focusing and acoustic communications in the surf zone," *J. Acoust. Soc. Amer.*, vol. 116, no. 4, pp. 2067–2080, Oct. 2004.

[8] A. Song, M. Badiey, H. C. Song, W. S. Hodgkiss, and M. B. Porter, "Impact of ocean variability on coherent underwater acoustic communications during the Kauai experiment (KauaiEx)," *J. Acoust. Soc. Amer.*, vol. 123, no. 2, pp. 856–865, Feb. 2008.
[9] D. Rouseff, M. Badiey, and A. Song, "Effect of reflected and refracted signals in coherent underwater acoustic communication: Results from the Kauai experiment (KauaiEx 2003)," *J. Acoust. Soc. Amer.*, vol. 126, no. 5, pp. 2359–2366, Nov. 2009.
[10] A. Song, M. Badiey, A. Newhall, J. Lynch, H. DeFerrari, and B. Katsnelson, "Passive time reversal acoustic communications through shallow-water internal waves," *IEEE J. Ocean. Eng.*, vol. 35, no. 4, pp. 756–765, Oct. 2010.
[11] M. Stojanovic, J. Catipovic, and J. G. Proakis, "Adaptive multichannel combining and equalization for underwater acoustic communications," *J. Acoust. Soc. Amer.*, vol. 94, no. 3, pp. 1621–1631, Sept. 1993.
[12] M. Stojanovic, J. Catipovic, and J. G. Proakis, "Phase-coherent digitial communications for underwater acoustic channels," *IEEE J. Ocean. Eng.*, vol. 19, no. 1, pp. 100–111, Jan. 1994.
[13] Y. R. Zheng, C. Xiao, T. C. Yang, and W.-B. Yang, "Frequency-domain channel estimation and equalization for shallow-water acoustic communications," *Elsevier J. Phys. Commun.*, vol. 3, pp. 48–63, Mar. 2010.
[14] J. Tao, Y. R. Zheng, C. Xiao, T. C. Yang, and W.-B. Yang, "Channel equalization for single carrier MIMO underwater acoustic communications," *EURASIP J. Adv. Signal Process.*, 2010, doi: 10.1155/2010/281769.
[15] M. Stojanovic, "Low complexity OFDM detector for underwater channels," presented at the MTS/IEEE OCEANS Conf., Boston, MA, Sep. 18–21, 2006.
[16] M. Stojanovic, "OFDM for underwater acoustic communications: Adaptive synchronization and sparse channel estimation," presented at the Int. Conf. Acoust., Speech, Signal Process., Las Vegas, NV, Apr. 2008.
[17] P. Ceballos and M. Stojanovic, "Adaptive channel estimation and data detection for underwater acoustic MIMO OFDM systems," *IEEE J. Ocean. Eng.*, vol. 35, no. 3, pp. 635–646, Jul. 2010.
[18] J. Huang, S. Zhou, and Z. Wang, "Robust initialization with reduced pilot overhead for progressive underwater acoustic OFDM receivers," in *Proc. MILCOM Conf.*, Nov. 2011, pp. 406–411.
[19] J.-Z. Huang, S. Zhou, J. Huang, C. R. Berger, and P. Willett, "Progressive inter-carrier interference equalization for OFDM transmission over time-varying underwater acoustic channels," *IEEE J. Sel. Topics Signal Process.*, vol. 5, no. 8, pp. 1524–1536, Dec. 2011.
[20] J.-Z. Huang, S. Zhou, J. Huang, J. Preisig, L. Freitag, and P. Willett, "Progressive MIMO-OFDM reception over time-varying underwater acoustic channels," presented at the Asilomar Conf. Signals, Syst., Comput., Pacific Grove, CA, Nov. 2010.
[21] B. Li, S. Zhou, M. Stojanovic, L. Freitag, and P. Willett, "Multicarrier communication over underwater acoustic channels with nonuniform Doppler shifts," *IEEE J. Ocean. Eng.*, vol. 33, no. 2, pp. 198–209, Apr. 2008.
[22] C. R. Berger, S. Zhou, J. Preisig, and P. Willett, "Sparse channel estimation for multicarrier underwater acoustic communication: From subspace methods to compressed sensing," *IEEE Trans. Signal Process.*, vol. 58, no. 3, pp. 1708–1721, Mar. 2010.
[23] T. Kang and R. A. Iltis, "Iterative carrier frequency offset and channel estimation for underwater acoustic OFDM systems," *IEEE J. Sel. Areas Commun.*, vol. 26, no. 9, pp. 1650–1661, Dec. 2008.
[24] G. Leus and P. A. V. Walree, "Multiband OFDM for covert acoustic communications," *IEEE J. Sel. Areas Commun.*, vol. 26, no. 9, pp. 1662–1673, Dec. 2008.
[25] T. Kang, H. C. Song, W. S. Hodgkiss, and J. S. Kim, "Long-range multi-carrier acoustic communications in shallow water based on iterative sparse channel estimation," *J. Acoust. Soc. Amer.*, vol. 128, no. 6, Dec. 2010.
[26] K. Tu, D. Fertonani, T. M. Duman, M. Stojanovic, J. Proakis, and P. Hursky, "Mitigation of intercarrier interference for OFDM over time-varying underwater acoustic channels," *IEEE J. Ocean. Eng.*, vol. 36, no. 2, pp. 156–171, Apr. 2011.
[27] J. Tao, Y. R. Zheng, C. Xiao, and T. C. Yang, "Robust MIMO underwater acoustic communications using turbo block decision-feedback equalization," *IEEE J. Ocean. Eng.*, vol. 35, no. 4, pp. 948–960, Oct. 2010.
[28] J. Tao, J. Wu, Y. R. Zheng, and C. Xiao, "Enhanced MIMO LMMSE turbo equalization: Algorithm, simulations and undersea experimental results," *IEEE Trans. Signal Process.*, vol. 59, no. 8, pp. 3813–3823, Aug. 2011.
[29] C. R. Berger, J. P. Gomes, and J. M. F. Moura, "Study of pilot designs for cyclic-prefix OFDM on time-varying and sparse underwater acoustic channels," presented at the MTS/IEEE OCEANS Conf., Santander, Spain, Jun. 2011.
[30] C. R. Berger, J. P. Gomes, and J. M. F. Moura, "Sea-trial results for cyclic-prefix OFDM with long symbol duration," presented at the MTS/IEEE OCEANS Conf., Santander, Spain, Jun. 2011.
[31] J. A. Tropp and A. C. Gilbert, "Signal recovery from random measurements via orthogonal matching pursuit," *IEEE Trans. Inf. Theory*, vol. 53, no. 12, pp. 4655–4666, Dec. 2007.
[32] D. Donoho, "Compressed sensing," *IEEE Trans. Inf. Theory*, vol. 52, no. 4, pp. 1289–1306, Apr. 2006.
[33] S. J. Wright, R. D. Nowak, and M. A. T. Figueiredo, "Sparse reconstruction by separable approximation," *IEEE Trans. Signal Process.*, vol. 57, no. 7, pp. 2479–2493, Jul.bv 2009.
[34] Z.-H. Wang, S. Zhou, J. Catipovic, and J. Huang, "A factor-graph based ZP-OFDM receiver for deep water acoustic channels," presented at the MTS/IEEE OCEANS Conf., Seattle, WA, Sep. 2010.
[35] J. Huang, S. Zhou, and P. Willett, "Nonbinary LDPC coding for multicarrier underwater acoustic communication," *IEEE J. Sel. Areas Commun.*, vol. 26, no. 9, pp. 1684–1696, Dec. 2008.
[36] S. Mason, C. R. Berger, S. Zhou, and P. Willett, "Detection, synchronization, and Doppler scale estimation with multicarrier waveforms in underwater acoustic communication," *IEEE J. Sel. Areas Commun.*, vol. 26, no. 9, pp. 1638–1649, Dec. 2008.
[37] D. A. Abraham and P. K. Willett, "Active sonar detection in shallow water using the page test," *IEEE J. Ocean. Eng.*, vol. 27, no. 1, pp. 35–46, Jan. 2002.
[38] K. Popat and R. W. Picard, "Cluster-based probability model and its application to image and texture processing," *IEEE Trans. Image Process.*, vol. 6, no. 2, pp. 268–284, Feb. 1997.
[39] X. Ma, C. Tepedelenlioğlu, G. B. Giannakis, and S. Barbarossa, "Non-data-aided carrier offset estimations for OFDM with null subcarriers: Identifiability, algorithms, and performance," *IEEE J. Sel. Areas Commun.*, vol. 19, no. 12, pp. 2504–2515, Dec. 2001.

Zhaohui Wang (S'10) received the B.S. degree from the Beijing University of Chemical Technology (BUCT), China, in 2006 and the M.Sc. degree from the Institute of Acoustics, Chinese Academy of Sciences (IACAS), Beijing, China, in 2009, both in electrical engineering. She is currently working toward the Ph.D. degree in the Department of Electrical and Computer Engineering at the University of Connecticut (UCONN), Storrs.

Her research interests lie in the areas of communications, signal processing and detection, with recent focus on multicarrier modulation algorithms and signal processing for underwater acoustic communications.

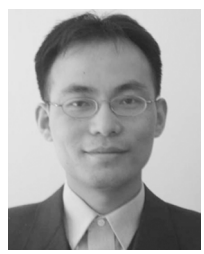

Shengli Zhou (SM'11) received the B.S. and M.Sc. degrees, both in electrical engineering and information science, from the University of Science and Technology of China (USTC), Hefei, in 1995 and 1998, respectively, and the Ph.D. degree in electrical engineering from the University of Minnesota (UMN), Minneapolis, in 2002.

From 2003 to 2009, he was an Assistant Professor with the Department of Electrical and Computer Engineering at the University of Connecticut (UCONN), Storrs, where he is currently an Associate Professor. He holds a United Technologies Corporation (UTC) Professorship in Engineering Innovation from 2008 to 2011. His general research interests lie in the areas of wireless communications and signal processing. His recent focus is on underwater acoustic communications and networking.

Dr. Zhou served as an Associate Editor for IEEE TRANSACTIONS ON WIRELESS COMMUNICATIONS from February 2005 to January 2007 and the IEEE TRANSACTIONS ON SIGNAL PROCESSING from October 2008 to October 2010. He is currently an Associate Editor for the IEEE JOURNAL OF OCEANIC ENGINEERING. He received the 2007 ONR Young Investigator award and the 2007 Presidential Early Career Award for Scientists and Engineers (PECASE).

James C. Preisig (S'79–M'80) received the B.S. degree in electrical engineering from the United States Coast Guard Academy, New London, CT, in 1980, the S.M. and E.E. degrees in electrical engineering from the Massachusetts Institute of Technology, Cambridge, in 1988, and the Ph.D. degree in electrical and ocean engineering from the Massachusetts Institute of Technology/Woods Hole Oceanographic Institution (WHOI) Joint Program in Oceanography and Oceanographic Engineering, Cambridge, MA, in 1992.

He was a Postdoctoral Investigator at WHOI from 1992 to 1994 and a Visiting Assistant Professor at Northeastern University, Boston, MA, from 1994 to 1997. Since July 1997, he has been on the scientific staff of the Department of Applied Ocean Physics and Engineering, WHOI, where he is currently an Associate Scientist with tenure. His research interests are in the areas of adaptive signal processing, system identification, underwater acoustic propagation modeling, underwater acoustic communications, and numerical optimization.

Dr. Preisig is the recipient of the 1999 U.S. Office of Naval Research Ocean Acoustics Young Faculty Award and is a member of the Acoustical Society of America's Underwater Acoustics and Signal Processing Technical Committees. He is also an Associate Editor of the IEEE JOURNAL OF OCEANIC ENGINEERING and served as a member of the IEEE Sensor Array and Multichannel Signal Processing Technical Committee from 1998 to 2004.

Krishna R. Pattipati (S'77–M'80–SM'91–F'95) received the B.Tech. degree in electrical engineering with highest honors from the Indian Institute of Technology, Kharagpur, in 1975, and the M.S. and Ph.D. degrees in systems engineering from the University of Connecticut, Storrs, in 1977 and 1980, respectively.

From 1980 to 1986, he was employed by ALPHATECH, Inc., Burlington, MA. Since 1986, he has been with the University of Connecticut, where he is currently the UTC Professor of Systems Engineering in the Department of Electrical and Computer Engineering. He has served as a consultant to Alphatech, Inc., Aptima, Inc., and IBM Research and Development. He is a cofounder of Qualtech Systems, Inc., a small business specializing in intelligent diagnostic software tools. His current research interests are in the areas of agile planning in dynamic and uncertain environments, diagnosis and prognosis techniques for complex system monitoring, and predictive analytics for threat detection. He has published over 400 articles, primarily in the application of systems theory and optimization (continuous and discrete) techniques to large-scale systems.

Dr. Pattipati was selected by the IEEE Systems, Man, and Cybernetics Society as the Outstanding Young Engineer of 1984, and received the Centennial Key to the Future award. He was elected a Fellow of the IEEE in 1995 for his contributions to discrete-optimization algorithms for large-scale systems and team decision making. He has served as the Editor-in-Chief of the IEEE TRANSACTIONS ON SYSTEMS, MAN, AND CYBERNETICS—PART B: CYBERNETICS from 1998 to 2001, Vice-President for Technical Activities of the IEEE SMC Society from 1998 to 1999, and as Vice-President for Conferences and Meetings of the IEEE SMC Society from 2000 to 2001. He was corecipient of the Andrew P. Sage award for the Best SMC Transactions Paper for 1999, the Barry Carlton Award for the Best AES Transactions Paper for 2000, the 2002 and 2008 NASA Space Act Awards for A Comprehensive Toolset for Model-based Health Monitoring and Diagnosis, the 2003 AAUP Research Excellence Award, and the 2005 School of Engineering Teaching Excellence Award at the University of Connecticut. He also won the Best Technical Paper Awards at the 1985, 1990, 1994, 2002, 2004, 2005, and 2011 IEEE AUTOTEST Conferences, and at the 1997 and 2004 Command and Control Conferences.

Peter Willett (F'03) received the B.A.Sc. (engineering science) from the University of Toronto, Ontario, Canada, in 1982 and the Ph.D. degree from Princeton University, Princeton, NJ, in 1986.

He has been a faculty member at the University of Connecticut, Storrs, ever since, and since 1998 a Professor. His primary areas of research have been statistical signal processing, detection, machine learning, data fusion and tracking. He has interests in and has published in the areas of change/abnormality detection, optical pattern recognition, communications, and industrial/security condition monitoring.

Dr. Willett is Editor-in-Chief for the IEEE TRANSACTIONS ON AEROSPACE AND ELECTRONIC SYSTEMS and, until recently, was Associate Editor for three active journals: the IEEE TRANSACTIONS ON AEROSPACE AND ELECTRONIC SYSTEMS (for Data Fusion and Target Tracking) and the IEEE TRANSACTIONS ON SYSTEMS, MAN, AND CYBERNETICS, PARTS A and B. He is also Associate Editor for the *IEEE Aerospace and Electronics Systems Magazine* (AES Magazine), Editor of the AES Magazine's periodic Tutorial issues, Associate Editor for ISIF's electronic *Journal of Advances in Information Fusion*, and a member of the Editorial Board of the *IEEE Signal Processing Magazine*. He has been a member of the IEEE AESS Board of Governors since 2003. He was General Co-Chair (with S. Coraluppi) for the 2006 ISIF/IEEE Fusion Conference in Florence, Italy; Program Co-Chair (with E. Santos) for the 2003 IEEE Conference on Systems, Man, and Cybernetics, Washington DC; and Program Co-Chair (with P. Varshney) for the 1999 Fusion Conference, Sunnyvale, CA.